SCIENCE CHINA
Information Sciences

• MOOP •

October 2024, Vol. 67, Iss. 10, 204201:1–204201:3
https://doi.org/10.1007/s11432-024-4154-5

Underwater RGB-D imaging system with millimetric precision

Yajun GAO[1,2,3], Yang CONG[4*], Xu TANG[1,2] & Mingxue LI[1,2,3]

[1]*State Key Laboratory of Robotics, Shenyang Institute of Automation, Chinese Academy of Sciences, Shenyang* 110016*, China;*
[2]*Institutes for Robotics and Intelligent Manufacturing, Chinese Academy of Sciences, Shenyang* 110016*, China;*
[3]*University of Chinese Academy of Sciences, Beijing* 100049*, China;*
[4]*College of Automation Science and Engineering, South China University of Technology, Guangzhou* 510640*, China*

Received 28 January 2024/Revised 9 May 2024/Accepted 10 July 2024/Published online 20 September 2024

In recent years, underwater fine three-dimensional reconstruction technology has emerged as a focal point in research, exhibiting extensive potential applications, particularly in underwater archaeology and resource exploration [1, 2]. However, the application of existing technologies in underwater settings is confronted with certain limitations. Some sensors, such as cameras, possess the capability to capture color information, while others, like sonar and structured light, are adept at acquiring depth information [3–5]. Nevertheless, the absence of a technique to effectively integrate these two sets of information hinders the achievement of highly faithful representations of underwater scenes. We aim to present targets as if they were revealed in front of observers after the removal of water, facilitating the precise capture of texture and color in underwater environment. Undoubtedly, the application of these technologies in underwater settings necessitates addressing challenges such as light attenuation, refraction, and color distortion [6–8].

To address the aforementioned challenges, we propose a millimeter-level underwater RGB-D imaging system, referred to as URGB-D. Specifically, this method focuses on the precise calibration of the system, acquisition of three-dimensional point clouds, and accurate mapping of colors. Our primary contributions encompass three key aspects:

• We propose a novel algorithm for underwater RGB-D refraction 3D reconstruction, which establishes a structured light model tailored for underwater refractive conditions. By incorporating the pose of the refraction camera, line structured light data, color information, and the position of the rotational platform, we achieve fine modeling of underwater targets, with reconstruction accuracy reaching the millimeter scale.

• We propose a simplified calibration process that only requires capturing one image underwater, with the remaining calibration performed in air. Compared with the calibration methods of the existing state-of-the-art models, our proposed method eliminates the necessity of underwater calibration of structured light and rotating platform parameters and improves the efficiency of calibration.

• We construct a prototype for experimentation with various underwater targets to assess the effectiveness of the proposed method. The experimental results demonstrate that our approach can recover dense RGB-D point clouds while maintaining high robustness.

Framework. The algorithm framework of the proposed URGB-D imaging system is shown in Figure 1. The framework of the algorithm includes three main processes: (1) Calibration: This process involves calibrating camera internal parameters, refraction camera model, structured light sensor and rotating platform. (2) Laser line processing: This phase encompasses intricate computational procedures, commencing with the extraction of laser stripe centroids, subsequently facilitating the computation of their corresponding three-dimensional coordinates in the world coordinate system based on pixel coordinates. (3) Color mapping: This process calculates the rotation matrix corresponding to each frame of the laser stripe image, thereby mapping discrete three-dimensional points to the color image to obtain color information. A further detailed explanation of these individual components is provided below to facilitate a comprehensive understanding of the algorithm.

Calibration. The flowchart of the calibration process is shown in Figure 1(c). Here we introduce it in sequence as follows.

(1) Camera internal parameters. We collect a series of images in the air based on the pinhole camera model to calculate the camera internal parameters.

(2) Refraction camera model. We propose a refractive camera model that accounts for the change in the optical path when light passes through the "water-glass-air" medium interface. The specific alteration in angle is determined by the refractive indices of the respective media. Fixing the position of the camera and checkerboard, and capturing an image in air and in water, we can calculate the parameters of the refraction camera model: the distance from the camera's optical center to the glass d_0 and the glass's normal vector n. Subsequently, we model light transmission based on Snell's law using these parameters.

(3) Structured light sensor calibration. We assume the line laser is projected perpendicular to the glass, which can be represented by a plane equation, i.e., $Z = AX + BY + D$. We capture a series of checkerboard images with and with-

* Corresponding author (email: congyang81@gmail.com)

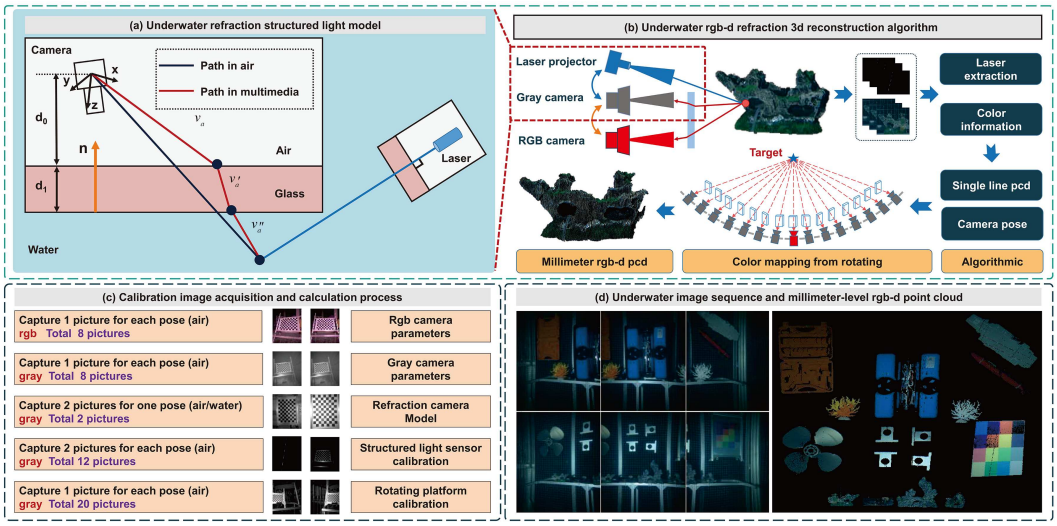

Figure 1 (Color online) Illustration of an underwater RGB-D imaging system with millimeter-level precision. (a) Underwater refraction structured light model; (b) underwater RGB-D refraction 3-D reconstruction algorithm; (c) calibration image acquisition and calculation process; (d) underwater image sequence and millimeter-level RGB-D point cloud.

out laser stripes and fit a plane based on the calculated 3D coordinates.

(4) Rotating platform calibration. Calibrating the rotating platform involves computing the matrix $[R, T]$ representing the camera's optical center relative to the center of rotation. We secure the equipment and calibration board while driving the motor to capture a series of images of the calibration board. Utilizing the PNP algorithm allows for the reverse calculation of the camera's position and orientation, fitting them as points along an arc. From this arc, the center and radius are determined, which can be translated into the rotation-translation matrix $[R, T]$.

Laser Line Processing. Diverging from the principles of structured light in air, our approach initiates from extracting two-dimensional points from laser stripe images. Leveraging a refractive camera model, we perform reverse calculations of light transmission paths to determine their intersection with the light plane, thereby obtaining precise three-dimensional coordinates. For a single image, this process takes approximately 50 milliseconds. Furthermore, in processing laser stripe images, we employ the Stegger algorithm to effectively extract line centers. The specific equations are as follows, $\boldsymbol{v_a}''$,$\boldsymbol{v_a}'$,$\boldsymbol{v_a}$ are the rays of a pixel, $\alpha_1, \beta_1, \alpha_2, \beta_2$ are refraction coefficients associated with the medium,

$$\begin{cases} \boldsymbol{v_a}'' = \alpha_2 \boldsymbol{v_a}' + \beta_2 \boldsymbol{n} = \alpha_2 \left(\alpha_1 \boldsymbol{v_a} + \beta_1 \boldsymbol{n}\right) + \beta_2 \boldsymbol{n}, \\ aX + bY + cZ + d = 0. \end{cases} \tag{1}$$

Color mapping. We compute the rotation matrices corresponding to the images using position information recorded by encoders. This process facilitates the mapping of discrete three-dimensional points onto the color image for acquiring color information. Specifically, the intrinsic matrix of the color camera is denoted as K, the extrinsic matrices of both cameras as M_0, the rotational matrix from the gray camera to the center of rotation as M_g, the color camera as M_c. Additionally, the rotation angles corresponding to the gray and color images are denoted as ϕ and φ , respectively, with their respective rotation matrices as M_ϕ and M_φ,

$$(u, v, 1, 1)^{-1} = K \cdot M_\varphi^{-1} \cdot M_\phi \cdot M_c \cdot M_0 \cdot (x, y, z, 1)^{-1}, \tag{2}$$

where $(x, y, z, 1)^{-1}$ represents the 3-D coordinates corresponding to a point in the laser stripe. According to Eq.(2), it can be mapped onto the color image to acquire color information. $(x^{'}, y^{'}, z^{'}, 1)$ is established in the world coordinates with the center of rotation, ultimately resulting in an RGB-D point cloud of the underwater scene with coordinates $(x^{'}, y^{'}, z^{'}, r, g, b)$,

$$(x^{'}, y^{'}, z^{'}, 1) = M_\phi \cdot M_g \cdot (x, y, z, 1)^{-1}. \tag{3}$$

Experimental setup. The gray camera and the laser projector are synchronized through hardware triggering, forming the structured-light system to acquire underwater laser stripe images. The color camera is synchronized with LED to capture underwater color images. The rotating mechanism drives at a speed of 0.5 degrees per second, with both grayscale and color images having a resolution of 2448×2048. The grayscale image frame rate is 15 fps, while the color image frame rate is 1 fps. All components are encapsulated in a watertight aluminum alloy casing, capable of withstanding pressures at depths of up to 100 meters.

Experiments and analysis. We present a comparative analysis between our algorithm and the latest algorithms regarding the errors in plane and shape fitting, as shown in Figure 1(d) and Table 1. Specifically, to examine the impact of working distance and turbidity on our system, quantitative assessments were carried out on workpieces, propellers, and ship models under different distances and turbidity levels. Analysis of errors in X, Y, Z, and angles indicates millimeter-level reconstruction accuracy achieved by our system. For different turbidity environments, and the measuring distance is about 1500 mm. With the increase of distance and turbidity, the measurement error increases gradually. Furthermore, evaluations based on shape fitting and color quantification metrics (UCIQE and UICM) demonstrate favorable performance of our algorithm, showing a certain degree of robustness to turbidity. Overall, experimental findings confirm the capability of our system to capture finer color details and clearer geometric shapes. Notably, textual information on ship models in the reconstructed point cloud is perceptible. However, deviations between color and ground truth exist due to the influence of color attenuation

Table 1 Errors in plane and shape fitting among various algorithms, alongside a quantitative comparison of the reconstruction performance of our algorithm at different distances and levels of turbidity

Errors of plane fitting			Errors of shape fitting		
Method	Mean (mm)	Standard deviation (mm)	Method	Mean (mm)	Standard deviation (mm)
Pinhole Model (air)	0.70	0.52	Pinhole Model (air)	6.11	5.08
Pinhole Model (water)	0.12	0.09	Pinhole Model (water)	1.45	1.21
Elnashef [9]	0.23	0.15	Elnashef [9]	0.70	0.36
Chen [10]	0.19	0.14	Chen [10]	1.48	1.22
Ours	**0.08**	**0.05**	Ours	**0.58**	**0.25**

3-D Reconstruction accuracy in water at different distances

Distance (mm)	Object	Error in Z axis (mm)	Error in X axis (mm)	Error in Y axis (mm)	Error in angle (°)
1500	Workpiece	0.43	1.31	1.20	0.65
	Propeller	0.52	1.36	1.46	0.73
	Ship model	0.68	1.35	1.67	0.69
2500	Workpiece	0.72	2.43	1.42	1.19
	Propeller	0.76	2.47	1.48	1.25
	Ship model	0.79	2.52	1.52	1.20
3500	Workpiece	1.08	3.41	1.66	2.24
	Propeller	1.13	3.38	1.72	2.34
	Ship model	1.16	3.42	1.69	2.35

3-D Reconstruction accuracy and color evaluation in different turbidity water

Turbidity	Object	RMSE (mm)	Average error (mm)	UCIQE	UICM
Low (1 NTU)	Workpiece	0.32	0.63	0.4570	2.3987
	Propeller	0.77	1.2	0.4084	2.4740
	Ship model	0.78	0.91	0.4852	2.6208
Medium (5 NTU)	Workpiece	0.35	1.01	0.3588	1.6063
	Propeller	1.05	1.45	0.3876	1.8150
	Ship model	1.18	1.45	0.3977	1.7403
High (10 NTU)	Workpiece	0.44	1.64	0.3127	1.3987
	Propeller	1.69	1.6	0.3272	1.4110
	Ship model	1.37	1.84	0.3056	1.5718

and noise on the reconstruction results.

Conclusion. We propose an underwater RGB-D imaging system named URGB-D, capable of comprehensively reconstructing the three-dimensional structure and color information of underwater objects with millimeter-level accuracy. Specifically, we propose an underwater RGB-D refraction 3D reconstruction algorithm and simplified calibration process. Experimental results conducted underwater validate the performance of the proposed method, demonstrating its capability to capture finer color details and clearer geometric shapes. In future work, we plan to introduce color correction techniques and a more refined refraction observation model to further enhance the accuracy of underwater three-dimensional reconstruction.

Acknowledgements This work was supported by the National Natural Science Foundation of China (Grant Nos. 62127807, 62225310).

Supporting information Videos. The supporting information is available online at info.scichina.com and link.springer.com. The supporting materials are published as submitted, without typesetting or editing. The responsibility for scientific accuracy and content remains entirely with the authors.

References

1 Cheng D, Shi H, Xu A, et al. Visual-laser-inertial SLAM using a compact 3D scanner for confined space. In: Proceedings of 2021 IEEE International Conference on Robotics and Automation (ICRA), 2021. 5699–5705
2 Cong Y, Gu C, Zhang T, et al. Underwater robot sensing technology: a survey. Fundam Res, 2021, 1: 337–345
3 Bodenmann A, Thornton B, Ura T. Generation of high resolution three dimensional reconstructions of the seafloor in color using a single camera and structured light. J Field Robot, 2017, 34: 833–851
4 Hu Y, Rao W, Qi L, et al. A refractive stereo structured-light 3-D measurement system for immersed object. IEEE Trans Instrum Meas, 2022, 72: 1–13
5 Duecker D A, Hansen T, Kreuzer E. RGB-D camera-based navigation for autonomous underwater inspection using low-cost micro AUVs. In: Proceedings of the 2020 IEEE/OES Autonomous Underwater Vehicles Symposium (AUV), 2020. 1–7
6 Akkaynak D, Treibitz T. Sea-Thru: a method for removing water from underwater images. In: Proceedings of the IEEE/CVF Conference on Computer Vision and Pattern Recognition, 2019. 1682–1691
7 Gu C, Cong Y, Sun G, et al. MedUCC: medium-driven underwater camera calibration for refractive 3-D reconstruction. IEEE Trans Syst Man Cybern-Syst, 2021, 52: 5937–5948
8 Palomer A, Ridao P, Forest J, et al. Underwater laser scanner: ray-based model and calibration. IEEE/ASME Trans Mechatr, 2019, 24: 1986–1997
9 Elnashef B, Filin S. Theory and closed-form solutions for three-and n-layer flat refractive geometry. Int J Comput Vis, 2023, 131: 877–898
10 Chen X. A closed-form solution to single underwater camera calibration using triple wavelength dispersion and its application to single camera 3D reconstruction. IEEE Trans Imag Process, 2017, 26: 4553–4561